RSC Advances

RSC Advances RSCPublishing

COMMUNICATION

Lithium Storage Improvement from Hierarchical Double-Shelled SnO$_2$ Hollow Spheres

Shilong Jing,[a] Feng Gu,[*,a,b] Junhua Kong,[b] Chunrong Ma,[a] Pooi See Lee,[*,b] and Chunzhong Li[*,a]

We have developed hierarchical double-shelled SnO$_2$ hollow spheres by a sequential template-engaged method, in which the loosened SnO$_2$ floccules are well-grown on the inside wall of the hollow spheres. The unique hierarchical structure could provide more active sites for Li-Sn alloying-dealloying reaction and fast insertion/extraction of Li$^+$ ion with superb conductivity, helping to store more lithium (2578 mAh g^{-1}) with great cycling stability.

Li-ion batteries (LIB) have attracted considerable interests as one of the dominant power sources for portable electronic devices due to their superior properties such as high energy density, long cycle life, no memory effect and environmental friendliness. To meet the growing need for higher capacity, tremendous efforts have been focused on developing alternative high-performance electrode materials for next generation LIBs, especially metal oxides due to their high theoretical capacitance, natural abundance and low cost.

SnO$_2$ has a high theoretical capacity of 782 mAh g^{-1}, more than twice that of the current used graphite (370 mAh g^{-1}). [1,2] However, upon lithium insertion/extraction within SnO$_2$, large and uneven volume change would result in electrode pulverization and electrical connectivity failure.[3] Hollow structures have been exploited to effectively to mitigate this problem due to the enhanced kinetics and structural stability for lithium storage. [4-16] The interior space allows volume variation upon insertion/extraction of lithium ions to be better accommodated and thus leads to improved cycling stability. Recently, considerable efforts have been devoted to the fabrication of SnO$_2$ hollow structures such as hollow nanospheres and nanoboxes based on the soft-/hard-template methods. [17-21] The shell of the hollow structures has been constructed precisely, hoping to form permeable thin walls to make lithium ion diffusion much easier by shortening the diffusion length. It should be noted that the interior space is particularly worthy to being further explored by filling with appropriate active materials to improve Li$^+$ ion storage capacity without impairing the electrode stability. For example, hollow core-shell mesospheres of crystalline SnO$_2$ nanoparticles developed by

Deng et al. demonstrated very high Li$^+$ storage capacities and improved electrochemical characteristics when used as the anode material in lithium ion test batteries.[22] The experimental values for the first-cycle discharge and charge capacities were 2358 and 1303 mAh g^{-1}, respectively, and kept nearly 800 mAh g^{-1} at the end of the 30th cycle. It has been reported that SnO$_2$ particles with mesoporous structure exhibit enhanced electrochemical properties in comparison with its bulk counterpart.[23] It can be expected that mesoporous SnO$_2$ would be particularly beneficial for the overall lithium storage capacity after being sealed inside. Herein, we described a facile template-engaged method to grow SnO$_2$ loose floccules (LAs) on the inner surface of SnO$_2$ hollow spheres (CH-SnO$_2$) to form hierarchical double-shelled SnO$_2$ hollow spheres to further improve the overall lithium storage capacity without impairing the structural stability. Due to their larger surface areas and larger number of lithium-storage sites, CH-SnO$_2$ exhibits improved electrochemical properties when evaluated as anode materials in LIBs.
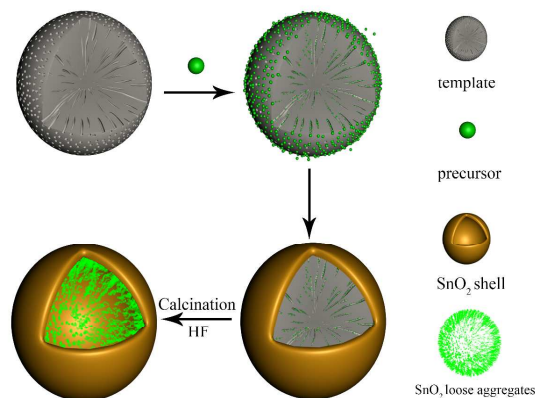
Scheme 1. Schematic illustration of the experimental procedure for the hierarchical double-shelled SnO$_2$ hollow spheres.

Scheme 1 illustrates the typical sequential template-engaged procedures for the synthesis of CH-SnO$_2$ hierarchical structures. SnO$_2$ nano-size floccules were firstly formed inside the channels of

mesoporous silica (MS) based on hydrolysis of potassium stannate. Subsequently, SnO_2-filled MS was used as template for the further deposition of SnO_2 layer on the outer surface of MS by further hydrolysis process. After the silica removal process, hierarchical loose floccules-encapsulated spherical SnO_2 hollow structure was obtained. Corresponding TEM images (Fig. S1) and more experimental details are provided in supporting information.
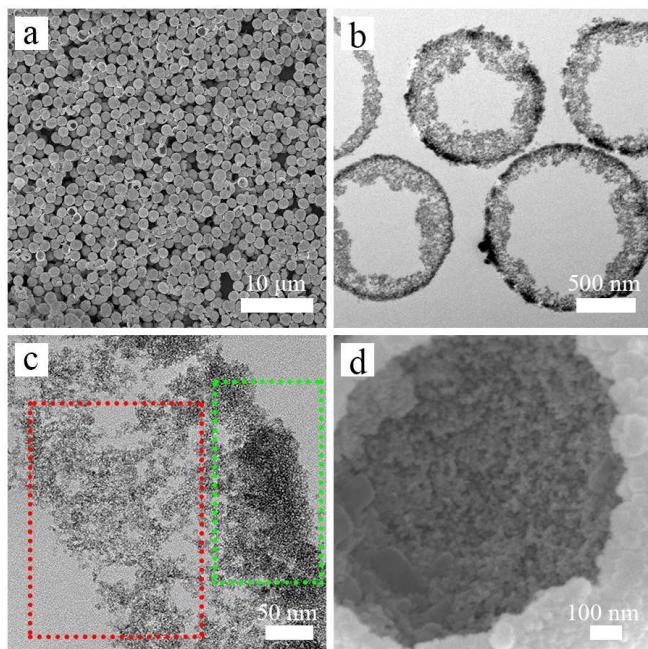
Figure 1. (a, b) SEM and cross-sectional TEM image of CH-SnO_2 particles. (c) HRTEM image showing the hierarchical double-shelled structure. (d) Selected SEM image of a broken CH-SnO_2.

The charged surface of MS determines the initial nucleation and confined growth owing to the electrostatic adsorption and the homogeneous nucleation could be suppressed totally during the hydrolysis reaction. The first hydrothermal process would lead to the formation of SnO_2 nano-size floccules within the channels with a very small size of the crystalline domains of ~2 nm, as derived from the HRTEM and the peak broadening in the XRD patterns shown in Figure S2. After the secondly hydrolysis and template removal processes, electron microscopy demonstrates obvious evidence that the hollow structure is highly hierarchical with mesoporous network that attaching to the inner surface of the dense shell (Fig. 1b and 1c). The shell was constructed by small nanoparticles and the shell thickness is about 100 nm. In virtue of the unique hollow structure and small crystallite size, the CH-SnO_2 particles possess a relatively large Brunauer-Emmett-Teller (BET) surface area of around 134 m^2 g^{-1}. From a broken CH-SnO_2 particle chosen randomly (Fig. 1d), it is clear that a fluffy layer could be observed on the inner surface of the shell. For comparison, hollow SnO_2 spheres without loose layer inside (H-SnO_2) derived directly from hydrolysis reaction taken solid silica sphere as template showed a rather smooth inner surface (Fig. S3).[24] Due to this special configuration, much better structural stability will be granted with consequently buffering the pulverization while increasing specific capacity of electrode when used as anode materials in LIBs.

Under the secondary hydrolysis process, the MS templates may act as the aggregation centers for the primary SnO_2 nanocrystals in view of the minimization of interfacial energy. However, excessive fast hydrolysis will be expected to cause formation of abundant irregular impurities inevitably and the secondary hydrolysis processes have to be controlled precisely when allowing the structure and morphology of the CH-SnO_2 particle being rationally controlled. Therefore, a proper concentration of precursor (potassium stannate) solution should be introduced into the reaction system to slow down the hydrolysis of Sn^{4+} so that nanoscale deposition can occur preferentially on the accessible surface of templates to construct conformal shells. In this work, the tin precursor concentration is optimized to be 8mM in case of templates concentration of 4.2 mg ml^{-1}, ensuring the precipitation of SnO_2 to take place at an appropriate rate. When the precursor concentration is insufficient (4mM) or excessive (16mM), aggregated SnO_2 particles and nodules-decorated spherical structures instead of conformal shells would be formed (Fig. S4). The latter could be attributed to the occurrence of homogeneous nucleation with the formation of SnO_2 nanocrystals in the system due to the excess precursor. Driven by energy minimization, the formed primary SnO_2 crystals may aggregate into bigger nanoparticles of ~ 200 nm, and then attached to SnO_2 shells through rotations caused by various interactions such as Brownian motion.
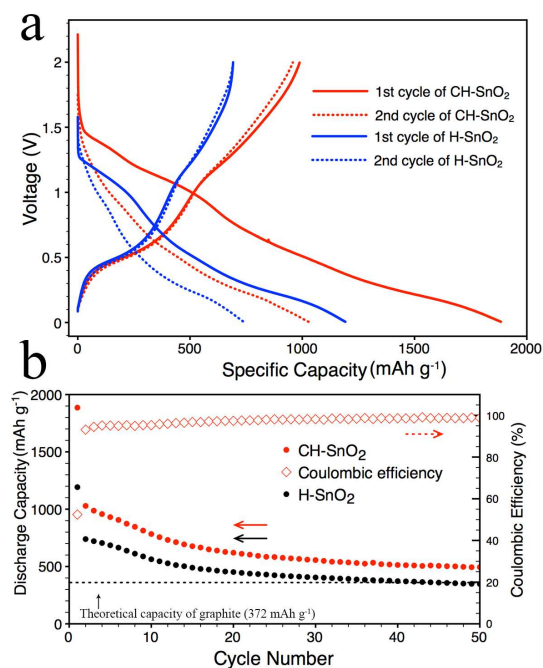
Figure 2. (a) Charge-discharge profiles of HC-SnO_2 and H-SnO_2. (b) The discharge capacities as a function of cycle numbers for CH-SnO_2 and H-SnO_2 at 100 mA g^{-1} and 5 mV - 2 V.

The electrochemical performances were evaluated by galvanostatic measurement. Figure 2a shows the first and second cycle charge-discharge voltage profiles for the CH-SnO_2 and H-SnO_2 samples at 100 mA g^{-1} within a cutoff window of 0.005-2 V. Two slope regions can be identified in the discharge process of the first cycle, which are in good agreement with those of SnO_2-based anodes, indicating the same electrochemical pathway. For CH-SnO_2, the discharge and charge capacities for the first cycle were estimated to be 1885 and

RSC Advances COMMUNICATION

1028 mAh g^{-1}, respectively (Fig. 2a). Such a high initial lithium storage capacity might be associated with the unique hierarchical structure with mesoporous network comprised by nano-size floccules. Compared with other hollow structures such as SnO_2 hollow nanosphere reported by Ding et al. and hollow core-shell mesospheres of crystalline SnO_2 nanoparticles by Deng et al., our results show better performance. [18,22] The apparently large disparity between charge and discharge capacities in the first cycle mainly ascribes to the initial irreversible formation of Li_2O, and other irreversible processes such as trapping of some Li^+ in SnO_2 LAs inside of the shells and electrolyte decomposition. [2,25-28]

Compared to H-SnO_2, CH-SnO_2 showed a sharp increase in Coulombic efficiency, from 52.4% to 94.5% after 3 cycles. From the second cycle onward, the capacity fades gradually to about 500 mAh g^{-1} over 50 cycles (Fig. 2b), which is much higher than the theoretical capacity of graphite. At the same discharge/charge rate (100 mA g^{-1}), it is clear that the initial discharge and charge capacities of H-SnO_2 are 1192 mAh g^{-1} and 739 mAh g^{-1}, respectively, much lower than the performance of CH-SnO_2. The specific discharge capacity at the end of the 50th cycle is 347 mAh g^{-1}, nearly 70% to the value of CH-SnO_2. Due to the equal mass of loose floccules network inside and SnO_2 shell, the first-time discharge and charge capacities derived from the SnO_2 LAs network are estimated to be as high as 2578 and 1317 mAh g^{-1}, respectively (calculation section in S.I.). Such high capacity improvement could be ascribed to the contribution of the mesoporous structure of the filled loose floccules: size in nanometer scale enables more active sites and solid attachment for super conductivity. The filled SnO_2 LAs could accommodate Li^+ more easily, and this would be strengthened after resistance was decreased more over by converting semiconducting SnO_2 into metallic Sn and forming Li_xSn alloys with Li. To further investigate stability of the hierarchical double-shelled structure, the electrode (without any removing of carbon black or PVDF) after 50 cycles has been examined. Although most of the CH-SnO_2 had expanded and some of them had collapsed with noticeable aggregation of SnO_2 nanoparticle floccules (Fig. S3-c), there were still unbroken spheres retained. The extended shadow (Fig. S3-d), compared to TEM images before cycles (Fig. S1-d), has clearly showed how intense was the electrochemical process during cycles.

The lithium insertion/extraction process in the CH-SnO_2 samples were further analyzed through cyclic voltammograms (CVs) at a scan rate of 5 mV s^{-1} in the potential range from 2.5 V to 0.005 V. As shown in figure 3a, three reduction peaks can be observed around 1.67, 1.23, 0.67 V, respectively, in the initial cathodic side. These peaks can be ascribed to the formation of the solid electrolyte interphase (SEI), the decomposition of SnO_2 to Sn and Li_2O nanocomposites, and finally the alloying reaction between Sn and Li, respectively. The first two reactions are irreversible and responsible for the large irreversible capacity of the first cycle. In the anodic side, one peak is observed at 0.68 V, indicating the highly reversible dealloying reaction of Li-Sn alloys. Another oxidation peak around 1.54 V is also observed for the CH-SnO_2, which is most likely due to the partial deformation of Li_2O. [29,30] Moreover, the CV curves increase in peak intensities in the first few cycles, suggesting the alloying of Li with Sn is gradual.
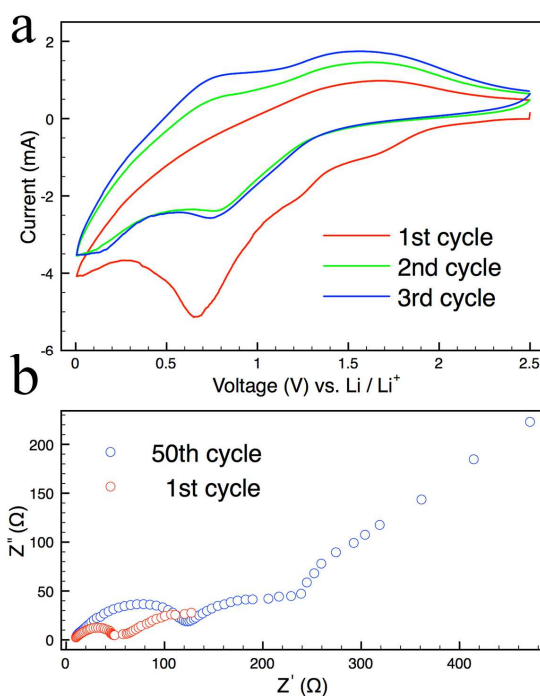
Figure 3. (a) Cyclic voltammograms of HC-SnO_2 at the first 3 cycles. (b) Nyquist plots obtained from the impedance spectroscopy of HC-SnO_2 before and after cycling for 50 cycles. AC voltage, 5 mV amplitude. Frequency range, 10 mHz to 100 kHz.

As the EIS results shown in figure 3b, the resistance of HC-SnO_2 was not very large even after 50 cycles. The increase of initial interfacial resistance (first semi-circle at high to middle frequency) and charge transfer resistance (second semi-circle or inclined line at middle to low frequency) could partially result from the formation of solid electrolyte interphase (SEI) and iterative lithium insertion / extraction. This is consistent with other reports. [30]

In summary, hierarchical loose floccules-encapsulated SnO_2 hollow spheres were prepared based on a facile sequential template-engaged method. This novel hierarchical structure exhibits a great improvement in electrochemical performance as an anode material for LIBs, such as higher capacity and good cycle performance in comparison with pure SnO_2 hollow spheres. The nano-size loose network inside would provide more active sites for Li-Sn alloying-dealloying reaction and fast insertion/extraction of Li^+ ion with superb conductivity, helping the hierarchical structure to store more lithium with great cycling stability, thereby, a prominent Li^+ ion storage capacity improvement was exhibited. This loose structure filling strategy has helped to enhance the performance of hollow structure remarkbly. The route could also be extended to prepare other metal oxide materials, which would have various applications in realm like energy storage, sensing and catalysis, to provide great performance.

Notes and references

[a]Key Laboratory for Ultrafine Materials of Ministry of Education, School of Materials Science and Engineering, East China University of Science and Technology, 130 Meilong Road, Shanghai 200237, China
[b]School of Materials Science and Engineering, Nanyang Technological University, 50 Nanyang Avenue, Singapore 639798

Fax: +86 21 64250624; Tel: +82 21 64252055

Email: czli@ecust.edu.cn; pslee@ntu.edu.sg; gufeng@ecust.edu.cn

1.   Y. Idota, T. Kubota, A. Matsufuji, Y. Maekawa, and T. Miyasaka, *Science*, 1997, **276**, 1395–1397.
2.   X. Lou, Y. Wang, C. Yuan, J. Lee, and L. Archer, *Adv. Mater.*, 2006, **18**, 2325–2329.
3.   Y. Xu, J. Guo, and C. Wang, *J. Mater. Chem.*, 2012, **22**, 9562–9567.
4.   V. Juttukonda, R. L. Paddock, J. E. Raymond, D. Denomme, A. E. Richardson, L. E. Slusher, and B. D. Fahlman, *J. Am. Chem. Soc.*, 2006, **128**, 420–421.
5.   H.-J. Ahn, H.-C. Choi, K.-W. Park, S.-B. Kim, and Y.-E. Sung, *J. Phys. Chem. B*, 2004, **108**, 9815–9820.
6.   J. Ba, J. Polleux, M. Antonietti, and M. Niederberger, *Adv. Mater.*, 2005, **17**, 2509–2512.
7.   Y. Wang, X. Jiang, and Y. Xia, *J. Am. Chem. Soc.*, 2003, **125**, 16176–16177.
8.   B. Cheng, J. M. Russell, Shi, L. Zhang, and E. T. Samulski, *J. Am. Chem. Soc.*, 2004, **126**, 5972–5973.
9.   L. Vayssieres and M. Graetzel, *Angew. Chem. Int. Ed.*, 2004, **43**, 3666–3670.
10. Z. W. Pan, *Science*, 2001, **291**, 1947–1949.
11. X. Wu, S. Zhang, L. Wang, Z. Du, H. Fang, Y. Ling, and Z. Huang, *J. Mater. Chem.*, 2012, **22**, 11151–11158.
12. L. Zhao, M. Yosef, M. Steinhart, P. Göring, H. Hofmeister, U. Gösele, and S. Schlecht, *Angew. Chem. Int. Ed.*, 2006, **45**, 311–315.
13. Z. R. Dai, Z. W. Pan, and Z. L. Wang, *J. Am. Chem. Soc.*, 2002, **124**, 8673–8680.
14. H. G. Yang and H. C. Zeng, *Angew. Chem. Int. Ed.*, 2004, **43**, 5930–5933.
15. Z. Zhong, Y.-D. Yin, B. Gates, and Y. Xia, *Adv. Mater.*, 2000, **12**, 206–209.
16. W. Shao, Z. Wang, Y. Zhang, J. Cui, W. Yu, and Y. Qian, *Chem. Lett.*, 2005, **34**, 556–557.
17. S. Han, B. Jang, T. Kim, S. M. Oh, and T. Hyeon, *Adv. Funct. Mater.*, 2005, **15**, 1845–1850.
18. S. Ding, J. S. Chen, G. Qi, X. Duan, Z. Wang, E. P. Giannelis, L. A. Archer, and X. W. Lou, *J. Am. Chem. Soc.*, 2010, **133**, 21–23.
19. P. Wu, N. Du, H. Zhang, C. Zhai, and D. Yang, *ACS Appl. Mater. Interfaces*, 2011, **3**, 1946–1952.
20. Z. Wang, D. Luan, F. Y. C. Boey, and X. W. Lou, *J Am Chem Soc*, 2011, **133**, 4738–4741.
21. Y. Liu, J. Dong, and M. Liu, *Adv. Mater.*, 2004, **16**, 353–356.
22. D. Deng and J. Y. Lee, *Chem. Mater.*, 2008, **20**, 1841–1846.
23. S. Yang, W. Yue, J. Zhu, Y. Ren, and X. Yang, *Adv. Funct. Mater.*, 2013, **23**, 3570–3576.
24. W. Stober, A. Fink, and E. Bohn, *J. Colloid Interface Sci.*, 1968, **26**, 62–69.
25. K. T. Lee, Y. S. Jung, and S. M. Oh, *J. Am. Chem. Soc.*, 2003, **125**, 5652–5653.
26. J. Ye, H. Zhang, R. Yang, X. Li, and L. Qi, *Small*, 2010, **6**, 296–306.
27. Y. Shi, B. Guo, S. A. Corr, Q. Shi, Y.-S. Hu, K. R. Heier, L. Chen, R. Seshadri, and G. D. Stucky, *Nano Lett.*, 2009, **9**, 4215–4220.
28. M.-S. Park, G.-X. Wang, Y.-M. Kang, D. Wexler, S.-X. Dou, and H.-K. Liu, *Angew Chem*, 2007, **119**, 764–767.
29. G. Xia, N. Li, D. Li, R. Liu, N. Xiao, and D. Tian, *Mater. Lett.*, 2011, **65**, 3377–3379.
30. J. Kong, Z. Liu, Z. Yang, H. R. Tan, S. Xiong, S. Y. Wong, X. Li, and X. Lu, *Nanoscale*, 2012, **4**, 525–530.